

Efficient Routing on Quantum Networks using Adaptive Clustering

Connor Clayton
University of Maryland
cbclayto@cs.umd.edu

Xiaodi Wu
University of Maryland
xwu@cs.umd.edu

Bobby Bhattacharjee
University of Maryland
bobby@cs.umd.edu

Abstract—We introduce QuARC, Quantum Adaptive Routing using Clusters, a novel clustering-based entanglement routing protocol that leverages redundant, multi-path routing through multi-particle projective quantum measurements to enable high-throughput, low-overhead, starvation-free entanglement distribution. At its core, QuARC periodically reconfigures the underlying quantum network into clusters of different sizes, where each cluster acts as a small network that distributes entanglement across itself, and the end-to-end entanglement is established by further distributing between clusters. QuARC does not require a-priori knowledge of any physical parameters, and is able to adapt the network configuration using static topology information, and using local (within-cluster) measurements only. We present a comprehensive simulation-based evaluation that shows QuARC is robust against changes to physical network parameters, and maintains high throughput without starvation even as network sizes scale and physical parameters degrade.

I. INTRODUCTION

Recent papers [1]–[4] have defined a framework for studying entanglement routing in quantum networks, leading to the development of several promising schemes. To date, the predominant family of concurrent quantum routing algorithms [2], [5]–[8] relies on entanglement swapping for entanglement distribution, often assuming that entanglement creation and swapping probabilities are known a-priori. Newer designs [3], [4], [9], [10] use multi-particle projective quantum measurements, referred to as *fusions*, that take advantage of multiple concurrent paths to enable entanglement over larger topologies. Both of these approaches have certain benefits and drawbacks.

Multi-path entanglement distribution protocols can provide very high throughput [2], [5], [7], [9], in terms of number of simultaneous successful entanglements, under favorable conditions. These protocols, however, are increasingly ineffective over larger network diameters, and rely heavily on sufficiently favorable physical conditions that must be known a-priori. Entanglement swapping protocols are also likely to “starve” longer-distance/larger-hop entanglement requests, as their effectiveness decreases rapidly with distance and hop count. More fundamentally, we show that the efficacy of these protocols is highly sensitive to the values of physical parameters and network size.

Fusion-based protocols, on the other hand, were designed to generate distance-independent entanglement [3], [4], and

are largely agnostic to network diameter. As long as the underlying topology provides sufficient connectivity, and the physical parameters are better than a critical threshold, these protocols can successfully provide end-to-end entanglement. These protocols, however, often cannot provide high entanglement throughput, either because they fail to take full advantage of multi-path routing [9] or they are restricted to servicing a single source-destination pair at a time [3], [4].

We introduce QuARC, Quantum Adaptive Routing using Clusters, a new quantum routing protocol that relies on adaptive clustering to address these shortcomings of previous protocols. QuARC does not require any time-varying global knowledge, nor does it assume the knowledge of physical parameters such as entanglement generation rates on any edge. Instead, QuARC uses a local measurement-based process to reconfigure the network periodically into fusion domains (or clusters), over which entanglement requests are served. Depending on (changing) physical parameters and entanglement request distribution, QuARC creates larger or smaller clusters, which are split or merged over time to maintain high performance with respect to throughput and request fulfillment latency.

QuARC is the first quantum routing protocol based on clustering, which is designed to strike a balance between providing high overall entanglement throughput and sustaining high success-rates for long distance entanglement requests. We evaluate QuARC using simulations, and study the effectiveness and robustness of clustering across a wide range of simulated physical parameters and network sizes. Importantly, we show that QuARC largely maintains the distance-independent nature of previous fusion-based protocols [3], [4], in that performance does not suffer (comparatively) as physical parameters degrade or network diameters increase. Simultaneously, we show that the performance of the best known multi-path entanglement routing protocols collapse (often to near-zero) under the same physical parameter shifts.

The rest of this paper is structured as follows: Section II provides a background on entanglement routing, including a discussion of related work. Section III presents QuARC’s design, followed by simulation evaluations in Section IV. We discuss QuARC’s limitations and avenues for future work, as well as a realistic distributed implementation in Section V; we conclude in Section VI.

II. BACKGROUND AND RELATED WORK

The use of traditional packet-switching in quantum networks is largely precluded by two fundamental quantum mechanical facts: general quantum messages cannot be copied [11] (the so called “no-cloning theorem”), and, without error correction, the information contained within these messages decays rapidly over time. Additionally, quantum information decays exponentially with distance [12], meaning that directly sending a long-distance quantum message fails with high probability, and attempting to resend that message is (in general) impossible due to the no-cloning theorem.

Instead, future large-scale quantum networks are expected to operate by *entanglement distribution*. Entanglement distribution uses two-particle entangled states known as *Bell pairs*. When two (distant) parties A and B are each in possession of one of the two particles in a Bell pair, we say that A and B *share entanglement*. This shared entanglement is a resource which A can use to send a single quantum bit, or *qubit*, to B through a process known as *quantum teleportation* [13]. The benefit of entanglement distribution (over direct transmission) is that, unlike general qubits, Bell pairs can be regenerated, the entanglement distribution attempt repeated until successful.

The success rate of sending a Bell state particle through fiber also decays exponentially with distance. Long distance networks therefore will rely on intermediate nodes known as *quantum repeaters* [12], [14]. A long-distance entanglement between A and B can be formed via an intermediate repeater C as follows: A and B each separately distribute entanglement with C. C then completes the long-distance A-B entanglement using *entanglement swapping* [15]–[18], essentially teleporting the two entanglements (A-C, C-B) locally. This process generalizes to multiple intermediaries, and such a sequence of entanglement swaps can be performed in parallel, which reduces latency and minimizes decoherence. Recent experiments have realized the foundational elements of multi-node entanglement swapping quantum networks [19], [20], and more limited quantum networks based on so-called “trusted repeaters” have been deployed at metropolitan scales and beyond for over a decade [21]–[26].

a) Network Model: This setting forms the basis for studying quantum networks: the network is modeled as a graph, where each node contains some number of *memory qubits*, and each edge contains one or more *quantum channels*. The number of quantum channels in an edge is known as that edge’s *width*. When two adjacent nodes each assign a qubit to a channel c , that channel can attempt to generate entanglement between those two qubits; this entanglement generation succeeds with probability p_c . We call a successful entanglement over a quantum channel a *link*. Previous works assume that p_c is entirely dependent on the length L of c by a network constant α , i.e., $p_c = e^{-\alpha L}$; however, we note that p_c may be affected by additional factors (e.g., cable splices [27]) and may also be time-varying due to, e.g., temperature change, wind speed, quantum device drift and re-calibration [27]–[29].

b) Routing Protocols using Entanglement Swapping:

This basic network model has been used to study physical

limits of entanglement generation, often focusing on specific physical topologies. Pirandola *et al.* uncover the fundamental limits of repeaterless quantum communication [12] as well as upper bounds on the transmission rates of arbitrary repeater-assisted quantum communication schemes [30]. Van Meter *et al.* [31] adapt classical path selection methods to account for quantum resource utilization. [32], [33] formulate entanglement distribution as linear programming problems. [34] propose a decentralized, hierarchical routing scheme. Numerous works analyze routing on special topologies such as chains, rings, grids, and trees [1], [35]–[40].

Expanding on these fundamental ideas, entanglement routing algorithms have been developed for the more general setting in which concurrent source-destination pairs must be serviced on an arbitrary network topology. Shi and Qian [2] developed the first of these, proposing a comprehensive model of the entanglement routing problem and corresponding algorithms for throughput maximization. Zhang *et al.* [5] extend [2] to more efficiently utilize local link state information, and Zhao and Qiao [7] demonstrate that global access to link state information can also improve throughput over [2]. [8], [41] consider request scheduling for improved fairness. Several works examine entanglement routing in various related settings, including under noisy link generation [6], time multiplexing [42], [43], and non-homogeneous time slots [44].

A. Fusion-based Entanglement Routing

Recently, a generalization of entanglement swapping which acts on more than two qubits has been studied in the context of quantum network routing [1], [3], [4], [9], [10], [45]. Known as *n-fusion*, or simply fusion, this operation acts on n qubits and “fuses” the entanglement stored in these qubits’ links into a larger multi-party entangled state (known as a GHZ state). To illustrate this effect, consider a node v which shares entanglement with n neighboring nodes: a successful fusion at v which acts on the relevant n qubits will result in a single, distributed, n -party entangled state shared by the n neighbors. Each node can perform a fusion on any number of successfully entangled qubits, and each fusion succeeds with probability q_n . This operation encompasses entanglement swaps, which are fusions on two qubits. Nodes have knowledge of which qubits are involved in successful links due to entanglement heralding [46], [47].

Analogously to a chain of entanglement swaps, fusions can be applied across a “network” of repeaters. While a sequence of swaps extends entanglement linearly, the effect of many fusions over a general network is that entanglement “spreads” through the network; as long as *any* path of successful links and fusions exists between the source and the destination, entanglement is distributed.

Figure 1 illustrates a scenario in which fusion-based routing out-performs swapping-based routing. Figure 1(a) shows an example of single-path routing: a single path of channels is selected to distribute entanglement, but one of the channels fails to produce a link (Figure 1(b)), and entanglement distribution is unsuccessful. Figure 1(c) demonstrates the utility of multi-

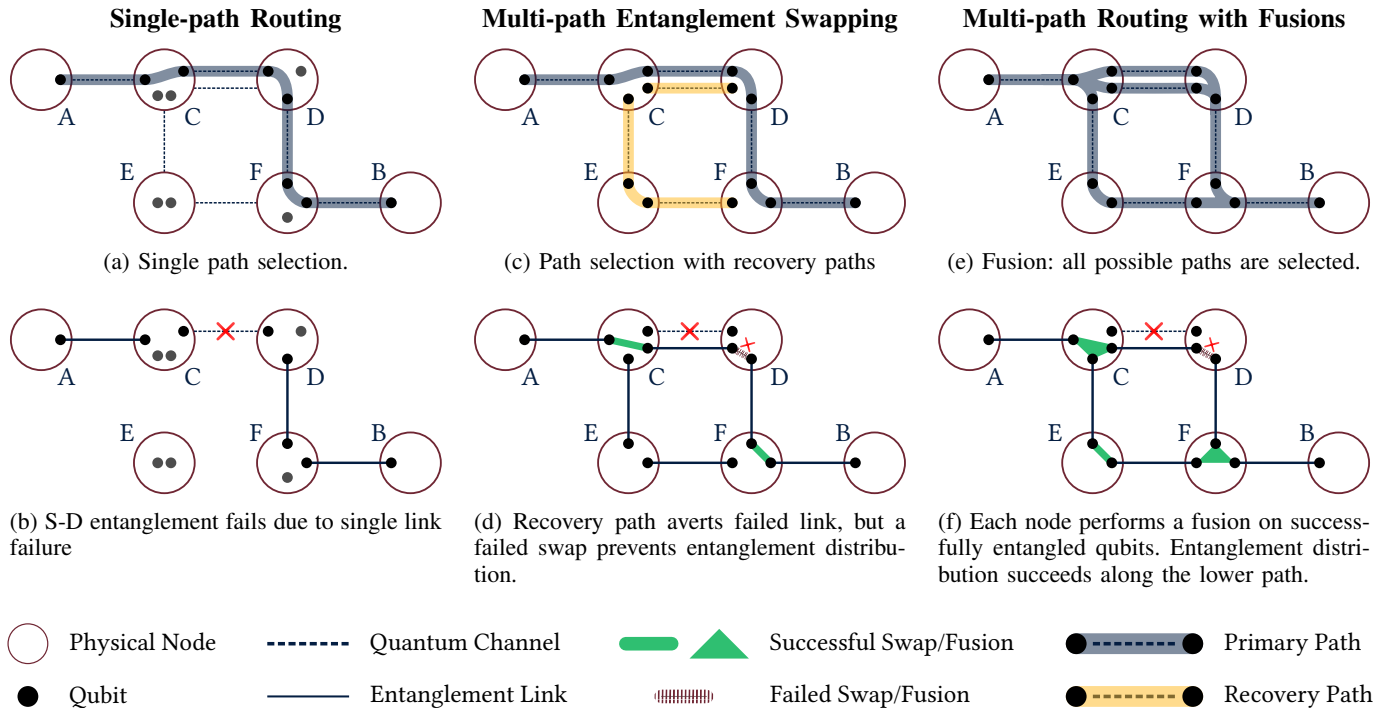


Figure 1: Comparison of different quantum routing approaches.

path routing, which allows “recovery edges” to be pre-selected to mitigate the effect of link failures. Figure 1(d) shows that such a scheme is able to withstand the failure of the same link by using a parallel recovery channel. In this example, the local swap at node D fails, and distribution is ultimately unsuccessful. Figure 1(e) demonstrates fusion, whereby *all* chosen channels comprise the routing “path.” The example shows how fusion-based protocols can withstand failures of both link establishment and local swaps, as either a successful path along $ACDFB$ or along $ACEFB$ would distribute entanglement; in this case the latter succeeded (Figure 1(f)).

Fusion-based protocols do not have to select the exact sequence of nodes that will lead to end-to-end entanglement distribution a-priori [1]. Assuming sufficient connectivity, fusion allows for attempting entanglement across “all” possible paths simultaneously: this observation forms the basis of a compelling result in [3], which shows that in 2-D square grid networks, a near unit entanglement distribution success rate is feasible, regardless of distance, as long as p and q are beyond a critical threshold. Follow up work [4] extends this protocol for links with lifetimes that exceed a single time slot and proposes a simple network partitioning scheme to improve the number of distributed entanglements between a single S-D pair. Kaur and Guha [45] study the square grid fusion protocol under noisy link generation. Sutcliffe and Beghelli [10] use fusions to construct a protocol for multi-partite entanglement distribution. [48], [49] analyze the impact of network topology and connectivity on entanglement rates over different distances for networks utilizing fusions. Zeng *et al.* [9] incorporate fusions into a concurrent, topology-agnostic routing protocol

by generalizing the methods in [2].

III. DESIGN

Figure 2 sketches entanglement routing in QuARC at a high level. At any given time, the network is partitioned into a set of clusters (Figure 2(a)). The input to QuARC is a set of source-destination pairs (S-D pairs) of nodes that request an end-to-end entanglement. Using Dijkstra’s shortest path algorithm, QuARC selects an end-to-end path over the graph induced by the clusters (Figure 2(b)); here, the individual nodes and edges within the chosen clusters define all possible entanglement paths between the source and destination. QuARC then assigns qubits to channels in a manner that distributes entanglement generation attempts across all edges within the chosen path of clusters in an approximately uniform manner. Each node then performs one or more fusions on its incident successfully entangled links to try to establish entanglement between the source and the destination.

Time in QuARC is divided into epochs. Data about each cluster’s effectiveness at distributing entanglement is collected throughout each epoch. Larger clusters, with more nodes, generally have a higher probability of being involved in a successful entanglement, as these provide more potential entanglement paths in our fusion-based scheme. The opposite is true for smaller clusters. While larger clusters increase the success probability of a given entanglement request, they may also decrease *overall* throughput since a cluster can only be involved in the service of a single S-D pair at any given time. (In the degenerate case, the entire network may be a single cluster, at which point, QuARC reduces to a protocol similar to that proposed in [3]). Thus the basic idea of QuARC is

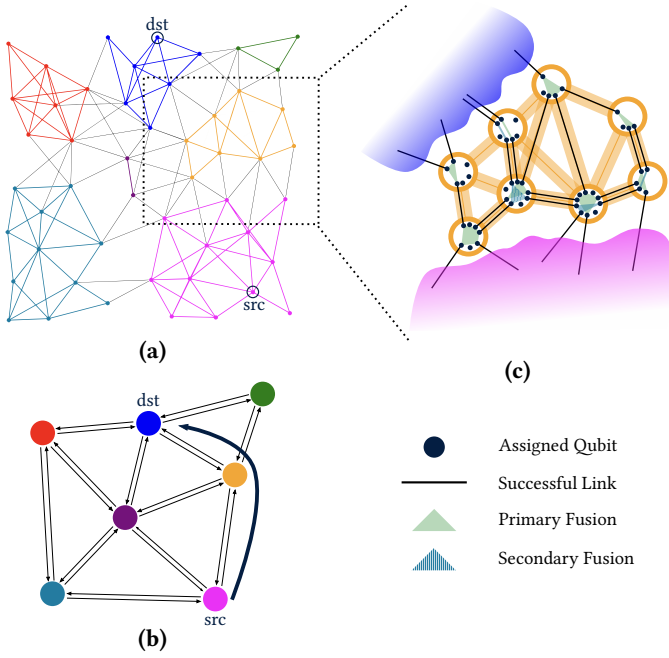


Figure 2: Routing in QuARC. (a) The network is partitioned into clusters. Nodes are colored by the cluster they belong to. (b) Shortest path routing over clusters. (c) Cluster nodes assign qubits to channels, attempt link generation, and perform fusions to route entanglement from the source to the destination.

to balance this tradeoff: create clusters just large enough to ensure end-to-end entanglements can be established, while small enough such that multiple entanglements can proceed simultaneously within the network.

Clusters are evaluated and potentially reconfigured at the end of each epoch. In particular, if a cluster’s rate of entanglement distribution is deemed “too low,” its size is increased by merging it with some number of nearby clusters. Conversely, if a cluster’s rate is deemed “too high,” its size is decreased by splitting it into multiple clusters.

In the rest of this section, we describe details of how clusters measure their performance and how clusters are re-configured, followed by a full description of QuARC.

a) Cluster Entanglement Passing Rate: Each time QuARC attempts to service an S-D pair, each cluster involved in this entanglement distribution attempt records whether a successful path of links and fusions was established from the previous cluster (or source, if contained within the cluster) to the next cluster (or destination). The proportion of successful attempts is logged per epoch as the cluster’s *entanglement passing rate*.

This process returns an estimate of the true expected entanglement passing rate for each cluster. This rate depends upon many factors, including the size of a cluster, the cluster’s internal connectivity, the cluster’s connectivity to adjacent clusters, the S-D request distribution, and link establishment rates under prevailing physical conditions. The latter is particularly important, as there is an interaction between how

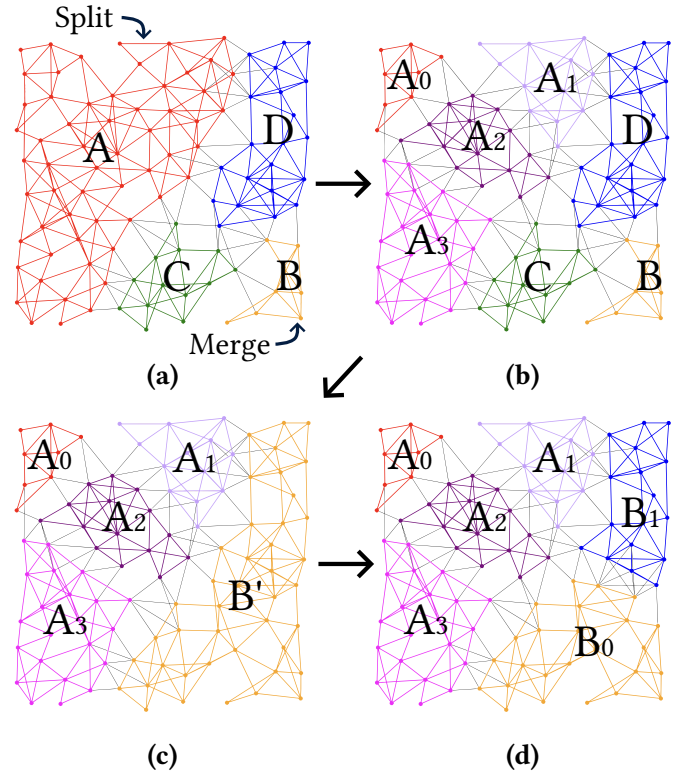


Figure 3: QuARC Cluster reconfiguration: cluster A (red) opts to split, and cluster B (orange) opts to merge. Panel (d) shows the final configuration.

quickly physical conditions change and epoch length. Epochs must be long enough for the estimator to gather useful data, but also not so long as to ignore material changes in physical parameters. It is possible that the cluster structure be re-configured manually if physical parameters or the S-D request distribution change drastically, but in QuARC, we rely entirely on the entanglement passing rate measurements to reconfigure clusters in response to these changes.

A. Cluster Reconfiguration

When should a cluster be split or merged? Consider a relatively large cluster, e.g., A in Figure 3(a), that has high entanglement passing rate. Intuitively, it seems that this cluster could be split, and the overall throughput in the network would increase as the split clusters would enable more concurrent routing requests and (ideally) retain a high enough entanglement passing rate. Splitting such a cluster may be beneficial in a relatively small network, but maintaining this cluster size may be required for high throughput in a larger network, as S-D request path lengths grow (and end-to-end entanglement establishment rate reduces exponentially). The utility of a cluster depends not only on its size, but also connectivity, both within and adjacent: the entanglement passing rate metric captures all of these parameters in terms of how “well” a cluster is performing locally. QuARC uses a dynamic split threshold that adds information about the network (its size, and optionally topology), along with a cluster’s current size

and entanglement passing rate, and only splits clusters that exceed this threshold.

A similar reasoning motivates our merge scheme: merging small, low entanglement passing rate clusters will likely improve throughput, but merging large clusters, which usually have higher entanglement passing rate, can reduce overall throughput. Analogously, we choose a dynamic merge threshold that again takes into account the same factors.

Our basic approach follows the intuition that large clusters (i.e., those containing many nodes) tend to have higher entanglement passing rates because they provide more potential entanglement paths, and vice-versa. To split a cluster, we partition it into k new clusters using the Girvan-Newman algorithm [50], which deterministically partitions a graph into a constant number of densely-connected communities. The Girvan-Newman algorithm is particularly appropriate because it maintains high connectivity for split clusters, which in turn, results in higher expected throughput for entanglement formation. Our results show that QuARC is relatively agnostic to small values of k ($\in [2, 5]$); we use $k = 4$ by default.

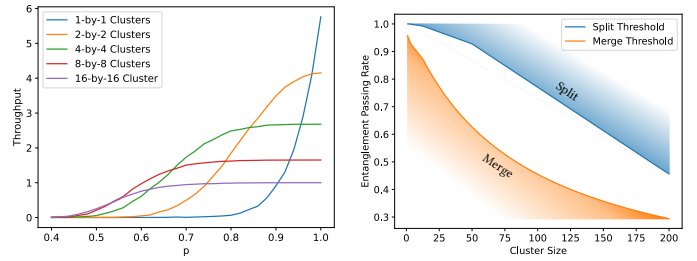
A possible merge procedure would be to merge k adjacent clusters. We opt for a somewhat more conservative approach, which enables a finer-set of cluster arrangements, without drastically reconfiguring the network every epoch. In particular, to grow a cluster, we select two of its neighbors and partition all nodes in these three clusters into two clusters using the Girvan-Newman algorithm (see Figure 3 (c-d)). This has the effect of eliminating one cluster from the network, and the use of the Girvan-Newman algorithm maintains well-connected clusters.

Figure 3 illustrates the process of cluster split and merge in QuARC. In this example, the large red cluster (labeled A) has opted to split, and the orange cluster (labeled B) has opted to merge. Panel (b) shows the result of a split (with $k = 4$) as output by the Girvan-Newman algorithm, splitting A into A0, A1, A2, and A3. To merge, cluster B identifies two neighbors, C and D, and these three clusters merge to form an intermediate cluster B' in panel (c). B' is then split into two, B0 and B1, in panel (d), completing the merge procedure.

1) *Threshold Selection*: Technically, a set of clusters should be merged iff the *incremental* percolation benefit from merging contributes more to overall throughput than is lost due to the reduced number of concurrent S-D requests that can be attempted. Similarly, a cluster should be split iff the reduction in the probability of establishing entanglement for a given S-D pair due to reduction in percolation is outweighed by the the gain in overall throughput due to increased number of concurrent S-D pairs.

Percolation benefits have been studied extensively in regular networks, including grid networks [51]. Percolation theory identifies critical connectivity thresholds beyond which grid networks provide S-D connectivity with high probability (and not otherwise). This observation was key in the development of fusion-based routing schemes [3], [4] that were, in part, an inspiration for QuARC.

Although existing theoretical percolation results apply only to a specific set of networks (e.g., [48], [49]) and do not



(a) Comparison of static clustering with varying p (b) Splitting and merging thresholds for $n = 200$

Figure 4: Threshold calculation.

directly apply to QuARC's network partitioning setting, we observe through simulation that such a configuration still demonstrates discrete thresholding behavior. Consider a 16×16 grid network with unit edge capacities, 4 qubits per node, and fixed q . A natural set of cluster configurations for this network is the set of square clusters with side lengths that are powers of two. Letting $p \in [0, 1]$ be constant and uniform for every channel, we can measure the expected throughput of each cluster configuration through simulation. Sweeping over p , we find that the optimal configuration indeed changes based on the value of p with distinct transition points (Figure 4(a)). Similar patterns emerge as we vary grid size.

Mapping these transition points to their corresponding average entanglement passing rates gives us optimal merging and splitting thresholds for 2-D grids. We generalize these thresholds to clusters of arbitrary sizes (non powers of 2) by plotting our known thresholds as a function of cluster size and linearly interpolating between cluster sizes (Figure 4(b)). We use the same procedure to generate thresholds for other regular ($N \times N$) 2-D grids. We linearly interpolate $N \times N$ grid thresholds to compute thresholds for other network sizes.

a) *Topology-specific Thresholds*: The 2-D grid derived thresholds can be used to refine thresholds for arbitrary (families of) topologies. For an arbitrary topology (say G), we derive a custom threshold as follows: we simulate QuARC on G starting with the 2-D grid thresholds, with varying *average* value of entanglement generation probability p .¹ We find the critical value p^* where using singleton clusters provides the same throughput as using QuARC with thresholds derived from the 2-D grids. We next simulate QuARC over G using p^* as the average entanglement passing rate, and document the entanglement passing rates e_i for the clusters QuARC creates at steady state. We compute G_t as the 75%-percentile value of e_i and set the topology-specific threshold to be $\min(G_t, 2D_t)$, where $2D_t$ is the threshold computed using the 2D-grid. We use the 75%-percentile value to be conservative in splitting.

We use the same procedure using p^* and the average entanglement passing rate of the singleton clusters to set the merge threshold. In our evaluation, we present results from both 2D-grid thresholds (scaled by network size) and using topology-specific thresholds as described here.

¹Note that in non-grid topologies, the p value changes by edge length.

b) *Escaping local minima:* Clusters in quarc can reach a state whereby the thresholds are insufficient for them to adapt, even though the cluster-structure around has changed significantly. To escape such “local” steady-states, we split a cluster C of size c if the majority of its neighbor clusters are less than size c/k . Recall that k is the split constant provided to the Girvan-Newman algorithm (a cluster splits into k clusters). We choose the c/k neighbor size threshold because when cluster C splits, it will create clusters of average size c/k .

B. QuARC Protocol

QuARC is initiated with a single cluster consisting of all nodes by default. At the end of each epoch, we examine the entanglement passing rate of each cluster. Here, we employ the cluster configuration protocol in Algorithm 1. Based on the thresholds described above, we mark each cluster for splitting if its entanglement passing rate is above the splitting threshold (or it meets the criterion for escaping a local minimum, see above) and otherwise mark it for merging if its entanglement passing rate is below the merging threshold (lines 1-3). We split those clusters marked for splitting as described above (lines 4-7). We then consider the clusters marked for merging in increasing order of entanglement passing rate. For each, we choose the two neighbors which induce the smallest Kemeny constant² [52] (line 10); if all relevant clusters are unmodified, we merge the chosen clusters using the merge protocol described above and mark the new clusters as modified (lines 11-15). If the cluster has exactly one neighbor (and it is unmodified), then we directly merge the two clusters into one.

1) *Routing Over Clusters:* Within each time slot, we select routing paths over clusters, assign qubits to channels, attempt entanglement generation, and perform fusions. Figure 2 shows the overall process, and we refer to this figure in our description below.

a) *Path Selection:* The S-D pairs in the request queue (e.g., in Figure 2(a), nodes *src* and *dst* request entanglement) are prioritized by their arrival times in order to minimize starvation. For each pair, a path of clusters is selected using Dijkstra’s algorithm over the graph induced by the clusters, where the weight of each (directed) edge is defined to be the size of the cluster on the tail end of the edge divided by the number of quantum channels between the two clusters (Figure 2(b)). This edge weighting prioritizes routes with high connectivity between clusters, while de-emphasizing routes that use excessive network resources. The selected clusters are removed from the graph and the process is repeated for the next S-D pair. If the remaining resources do not allow a path between an S-D pair, that pair is skipped (in the current time slot). Any skipped pair ages, and is likely to be selected earlier in subsequent rounds.

b) *Qubit Assignment:* Suppose the cluster path C_0, C_1, \dots, C_k is selected for a given S-D entanglement request. In QuARC, we do not assume that nodes can necessarily allocate qubits to all possible channels (i.e., nodes

²We choose the Kemeny constant as a measure of the connectedness of a component. Other choices, such as diameter, are also viable.

Algorithm 1 Adaptive Cluster Reconfiguration

Input: $G = \langle V, E, C \rangle$, current clusters $C = \{c_1, \dots, c_{|C|}\}$, sorted by entanglement passing rates $\{r_{c_1}, \dots, r_{c_{|C|}}\}$, merging and splitting thresholds m and s , respectively, constant k .

Output: New set of clusters (partitioning of V)

```

1:  $S \leftarrow \{c \in C \mid r_c \geq s(|c|)\}$  ▷ Clusters to split
2:  $S \leftarrow S \cup \{c \in C \mid \text{majority of } c\text{'s neighbors have size } < |c|/k\}$ 
3:  $M \leftarrow \{c \in C \setminus S \mid r_c \leq m(|c|)\}$  ▷ Clusters to merge
4: for  $c \in S$  do
5:    $d_1, \dots, d_k \leftarrow \text{Girvan-Newman}(c, k)$ 
6:   ▷ Split  $c$  into  $k$  components
7:    $C \leftarrow (C \setminus \{c\}) \cup \{d_1, \dots, d_k\}$ 
8:  $K \leftarrow \emptyset$  ▷ Set of merged clusters
9: for  $c \in M$  such that  $c$  has neighbors do
10:   $x_1, x_2 \leftarrow c\text{'s two neighbor clusters}^3$  that minimize induced
    Kemeny constant
11:  if  $c, x_1, x_2 \notin K$  then
12:     $d_1, d_2 \leftarrow \text{Girvan-Newman}(c \cup x_1 \cup x_2, 2)$ 
13:    ▷ Split three clusters into 2
14:     $C \leftarrow (C \setminus \{c, x_1, x_2\}) \cup \{d_1, d_2\}$ 
15:     $K \leftarrow K \cup \{c, x_1, x_2, d_1, d_2\}$ 
16: return  $C$ 

```

may be memory limited), and thus, QuARC needs to find a feasible assignment of qubits to channels. Qubit assignment proceeds in two steps: first, QuARC creates a union of all edges (\mathcal{E}) and a union of channels (\mathcal{C}) that are within C_i or between C_i and C_j , $i \neq j \in [0, k]$. Each edge $e_\ell \in \mathcal{E}$ is assigned a priority $a_\ell \in [0, 1]$ picked uniformly at random. Channels within each edge are assigned a priority $(a_\ell + i)$, where i is an integer index for the channel, starting from 0 for the first channel, 1 for the second, and so on. Channels are then sorted by priority and qubits are assigned sequentially in this sorted order, as long as each end of a channel has a free qubit remaining.

This method of allocating qubits ensures that, if possible, at least one qubit is allocated to every edge before any edge is assigned a second, and so on. However, this allocation of qubits is also essentially “random,” in that it does not take into account factors such as the shortest path between S and D, channel width of edges, number of parallel S-D paths that have received qubits, the values of p per edge or q per node, etc. This assignment serves to disperse qubits across the cluster. We discuss more enhanced qubit assignment strategies that can be used to optimize different potential metrics in Section V.

c) *Fusion Protocol:* Finally, all nodes follow a local fusion protocol similar to the protocol presented in [4]. Each node attempts entanglement generation according to its qubit assignments. All channels are given predetermined (arbitrary) ids. The node selects the successful link with the lowest id from each incident edge and attempts a fusion operation on these selected channels (labeled primary fusions in Figure 2(c)). It then repeats this process on the remaining links until no links remain (secondary fusions in Figure 2(c)). If

³In the edge case where c has exactly one neighbor x , we directly merge c and x into one cluster in a manner analogous to lines 11-15.

a selection of links would leave only one link remaining, that last link is included in the previous fusion attempt. We note that the primary fusions alone give the same result as fusing all links in the selected clusters at once, so the inclusion of secondary fusions only serves to increase the entanglement rate. All nodes send their fusion measurement results to the destination node, which computes whether or not the entanglement distribution was successful and applies the usual qubit corrections [3], [4].

IV. EVALUATION

We present an evaluation of QuARC, including its ability to adapt, and a comparison to current state-of-the-art quantum routing protocols.

A. Methodology

QuARC’s simulation code was custom written in Python, and allows the following parameters to be modified:

- Network topology: number and location of nodes, location and widths of edges
- Physical parameters: number of qubits per node, entanglement generation probability (p) per channel, and fusion success probability (q)

Once the physical parameters are set, the simulator can be configured to generate entanglement requests from configurable distributions. We generate S-D pairs uniformly at random unless otherwise noted. Once an S-D pair requests entanglement, the request remains in a global FIFO request queue until it is satisfied. The size of the request queue is configurable, and is set to 10 in our experiments unless otherwise noted. New entanglement requests are generated and appended to the request queue as existing ones are satisfied, which means that the request queue always contains ten requests (by default). Our choice of retaining failed entanglement requests differs from that of prior research [2], [9], where failed requests are discarded and not tried again. It is not clear whether it is reasonable to simply discard unsatisfied entanglement requests; this may depend on the specific quantum application. For example, if the task is to generate genuine quantum entanglement across the network [53], requests to entangle distant nodes cannot be simply discarded. We note, however, that it is also not clear that a satisfying a request after a long amount of time is necessarily useful; this again may be application-dependent. While QuARC prioritizes requests that were not satisfied in previous time slots, we do not impose this restriction on other protocols, which are allowed to optimize outstanding requests without limitation from our simulation framework. We ensure that the size of the request queue is never a limiting factor in any of the results presented below.

Our evaluation of QuARC is designed to address two broad questions: (1) How well can QuARC adapt to changing physical parameters and (2) How does QuARC’s performance compare to state of the art entanglement routing protocols? For the first, we present results comparing QuARC’s dynamic cluster configuration to fixed cluster arrangements, while varying p and q over time and space. For the latter, we compare QuARC

to Q-CAST [2] (a concurrent swapping-based protocol) and ALG-N-FUSION [9] (a concurrent fusion-based protocol). Our primary measures of performance are throughput (number of successful entanglements over time), latency (time before entanglement is successful) and starvation rates (fraction of entanglement requests that are unsuccessful). We note that there is a lack of consensus in how throughput ought to be measured in quantum settings: for instance, in many quantum routing evaluations [2], [5], [7], [9], if a S-D request is satisfied with three parallel entanglements, then the throughput for that particular request is considered to be 3. Such a configuration is useful if the application required three entanglements. Papers that focus on quantum network tasks, e.g., quantum distributed sensing network [54] or entanglement-based long-baseline interferometry [55], on the other hand, state that establishing all requested S-D entanglements is more important than counting the multiplicity of entanglements for each S-D pair. In our results, we count a request as satisfied if at least one S-D entanglement is achieved, and, by default, do *not* count the number of parallel entanglements in the measure of throughput. (We do discuss results with the “aggregate throughput” measure in select experiments.) A more realistic model would augment each request with the desired number of entanglements, an extension which would likely require changes to the design of QuARC and other protocols, which we leave as future work.

B. QuARC Adaptation

The initial question we wish to investigate is whether QuARC can efficiently adapt the underlying cluster structure as network parameters evolve. For this experiment, we use a 2-D grid network, as 2-D square clusters form a uniform configuration with high inter- and intra-cluster connectivity, and therefore constitute a natural baseline.

Figure 5(a-c) shows QuARC’s performance on a 16x16 grid, with a single channel per edge and no qubit limitations, as physical parameters p and q change. The x -axis is simulation time, and QuARC is started at time 0 with the default configuration of a single cluster. The cluster structure is not manually changed as p or q change. The other curves on the figure correspond to fixed cluster configurations, which provide high throughput for some combinations of p and q , but not others. Note that the 16x16 cluster configuration corresponds to a single cluster; on this topology, this configuration reduces to the 4-GHZ protocol described in [3].

Figure 5(a) corresponds to a situation where both p and q change abruptly but over long time intervals (every 5000 time slots) compared to cluster reconfiguration time (500 time slots). QuARC is able to reconfigure the clusters efficiently to track physical parameters, and reaches a stable state with performance equivalent to the best static cluster configuration (for that p/q) relatively quickly. We also experimented with changing p and q separately, and the results (not plotted) showed that QuARC is able to adapt efficiently.

Figure 5(b) shows a case where p decreases from 0.9 to 0.5 by 0.01 every 400 time slots. This situation is designed

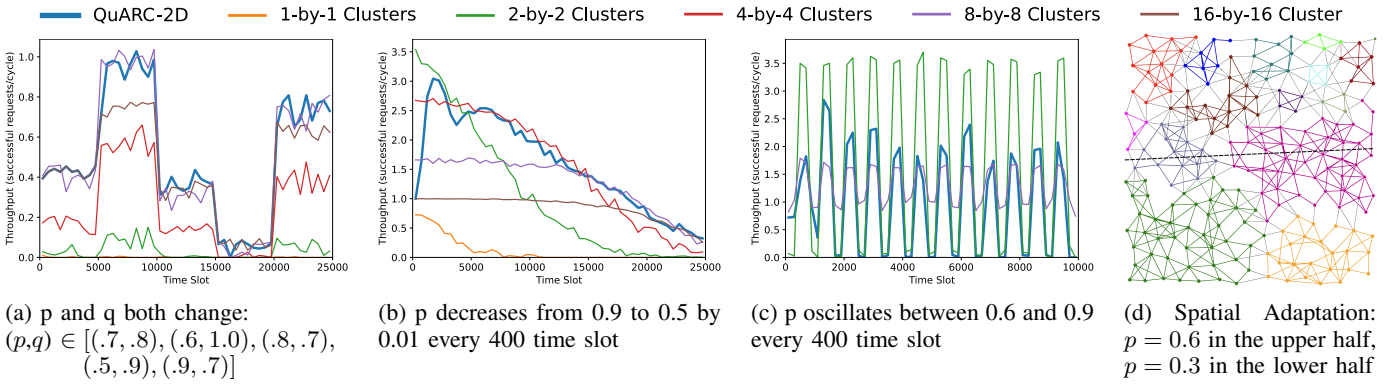


Figure 5: QuARC adaptation with changing physical parameters (p and q); (a-c) 16×16 grid network. (a) Sudden parameter shifts. (b) Gradual parameter decay. (c) Sharp parameter oscillation. (d) Spatially-varying parameters.

to reflect a case where link performance degrades over time, for instance due to changes in temperature or loss of synchronization between nodes [27], [29]. Note that in this scenario, network parameters change more frequently (every 400 time slots) than QuARC is able to reconfigure (500 time slots). QuARC is again able to provide high throughput, essentially equivalent to the best fixed cluster configuration. QuARC’s performance tends to lag slightly behind the best configuration, but is able to eventually find a suitable arrangement. Other experiments, not plotted, show that QuARC is able to similarly track increasing p .

Figure 5(c) explores an extreme scenario in which the network is unstable. Here, p oscillates between 0.6 and 0.9 every 400 time slots, and QuARC reconfigures every 500. As expected, QuARC is unable to track such rapid changes, but does provide some throughput when the entanglement probability rises. In practice, the epoch time used to initiate reconfiguration would have to be carefully selected based on how physical parameters evolve.

In addition to temporal adaptation, Figure 5(d) illustrates how QuARC’s clustering also adapts to spatial disparities. The figure shows the resulting cluster configuration in a scenario on a 200 node Waxman network [56] where channels in the top half of the topology have $p = 0.6$, and channels in the bottom half have $p = 0.3$ (other parameters follow the reference setting, described below). QuARC’s adaptation is able to detect this spatial disparity and, after convergence, form larger clusters in the bottom half of the network compared to the top.

C. Comparison of QuARC vs. existing protocols

In this section, we compare QuARC to two state-of-the-art quantum routing protocols, Q-CAST [2] and ALG-N-FUSION [9]. Unlike QuARC, both Q-CAST and ALG-N-FUSION utilize a-priori knowledge of all physical parameters; in particular, the values of p per channel and q per node. For these results, we follow the same topology generation method using the Waxman model [56] described in [2], and also used in [9]. As in [2], we give each topology an average degree

of 6 and we assign each node a number of qubits picked uniformly at random from the range $[10, 14]$ and each edge a width picked uniformly at random from the range $[3, 7]$. We follow the convention of denoting the average value of p across all channels as E_p . Each plotted point is an average of ten different simulation runs, with error bars showing the standard deviation of the mean.

a) *Protocol Implementations:* For these results, we used the simulator described in Section IV-A for QuARC. For Q-CAST, we used the publicly available simulation code [57] written in Kotlin. We did not change the provided code except to implement our request queueing (if necessary) and data collection. There was no publicly available code for ALG-N-FUSION: we implemented ALG-N-FUSION in Kotlin, based upon the description in the original reference [9]. All code used in these evaluations is publicly available [58].

b) *Throughput:* The throughput of each protocol under varying conditions is shown in Figure 6. Each plot shows throughput for a fixed value of $E_p \in \{0.3, 0.6\}$, with other parameters set as in [2] unless otherwise noted.

Figure 6(a) shows the throughput of QuARC, Q-CAST, and ALG-N-FUSION as a function of the number of nodes n in the topology when $E_p = 0.3$. Both QuARC-2D and QuARC-TS demonstrate the utility of clustering in this more constrained setting. At lower values of E_p , the throughput of Q-CAST and ALG-N-FUSION rapidly diminish to essentially zero with increasing network size, as most requests are starved, whereas both variants of QuARC are able to take advantage of the high path diversity inherent in clustering to sustain S-D entanglement success rates.

Figure 6(b) shows throughput as a function of network size in the more generous setting where $E_p = 0.6$. In the Q-CAST reference setting ($n = 100$, $E_p = 0.6$), Q-CAST and ALG-N-FUSION outperform QuARC-2D (QuARC with 2D-Grid thresholds and no knowledge of qubit availability). In this setting (and with $n = 50$), average path lengths are short, and the probability of a successful entanglement on a given edge is high $(1 - (1 - 0.6)^5) = 0.990$, assuming average channel width of five). This high entanglement generation

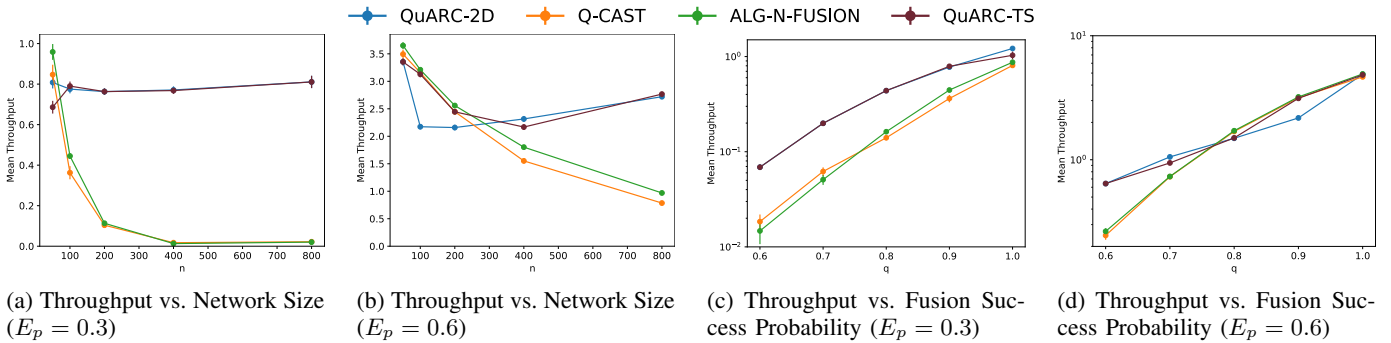


Figure 6: Throughput comparison with varying physical parameters and network size.

probability coupled with large number of available qubits leads to a resource-rich environment, enabling Q-CAST and ALG-N-FUSION to generate a comparatively high number of S-D entanglements. In such an environment, QuARC-2D is also able to generate a high entanglement rate, but the underlying clustering throttles throughput as it reduces the number of S-D pairs that QuARC-2D is able to attempt simultaneously. This disparity is eliminated when QuARC is run using topology-specific thresholds (QuARC-TS): the new thresholds, that are aware of both the underlying topology and qubit availability, increase the probability of splitting, resulting in higher throughput compared to QuARC-2D.

Despite their differences, a common picture emerges across both Figures 6(a-b) as network sizes increase: the throughput of Q-CAST and ALG-N-FUSION decrease dramatically while the throughput of QuARC is relatively stable. As network sizes increase, so do average path lengths, and the chance of a successful S-D entanglement decreases exponentially, even though individual edges still have a very high entanglement probability (about 0.99, as per above), and the chance of successful entanglement swap at a node is also high (0.9). Both QuARC variants, on the other hand, are relatively insulated from the increase in network size, as they can reconfigure the cluster structure to account for increased path lengths. As network sizes increase, both QuARC protocols automatically use larger clusters to effectively maintain a reasonable request success rate. (In results not plotted, we see that the *number* of clusters created by QuARC protocols remain relatively stable as network sizes increase, leading to increased cluster sizes for larger networks.)

Q-CAST and ALG-N-FUSION are similarly affected if the value of q changes. Figures 6(c-d) plot throughput (y -axis, log-scaled) for all three protocols for $E_p \in \{0.3, 0.6\}$ as q varies (x -axis) on the 100-node Q-CAST reference topology. As q decreases, end-to-end entanglement probabilities decrease exponentially for both Q-CAST and ALG-N-FUSION, while both QuARC variants are better able to compensate by creating larger clusters. While this result plots throughput performance for a 100 node graph, QuARC’s relative advantage increases substantially for larger networks (not plotted).

We discuss a few experiments not plotted due to space

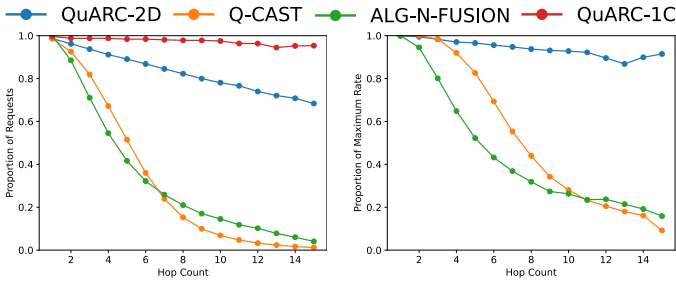
constraints. As discussed in Section IV-A, an alternate measure of throughput accounts for the number of parallel entanglements achieved, which can linearly increase throughput for successful entanglements. We refer to this measure as *aggregate throughput*. Experiments show that trends in aggregate throughput are similar to those in Figures 6(a-b), but with a modest relative boost for Q-CAST under favorable network conditions (small network size and high entanglement probability).

QuARC’s thresholds are derived using simulations that model a uniform distribution of S-D pairs requesting entanglement. We have explored QuARC’s sensitivity to request distribution, including modeling a “worst” case scenario for QuARC (least homogeneous request mix) by using a bimodal request distribution in which 50% of requests have a hop-distance that is 25% of the network diameter, and 50% of requests have a hop-distance that is 75% of the network diameter. We find that QuARC variants are also relatively unaffected by changes in request distribution, and maintain their advantage as network sizes increase, or as entanglement probabilities decrease.

Overall, these results are instructive, as they show:

- QuARC is able to maintain throughput performance as the network size increases across a wide range of p and q , as well as under non-uniform traffic patterns.
- The generic 2D-threshold version of QuARC can provide higher throughput than existing protocols on larger networks or with constrained values of p ; topology-specific QuARC maintains this advantage, and is able to better use network resources to perform on par with multi-path entanglement passing algorithms in smaller networks with high values of p and q .
- The performance of Q-CAST and ALG-N-FUSION is coupled to parameters such as entanglement generation probability p , fusion probability q , and network size. Performance degrades rapidly with network size or reduction in p or q values; as network sizes increase, in order to maintain performance, these protocols *require* that p , q also increase, or that channel widths increase.

c) Latency and Starvation: Along with throughput, latency (time before entanglement is established) and starvation



(a) Starvation: proportion of successful entanglement distribution attempts by distance

(b) Resource allocation bias: realized proportion of maximum success rate

Figure 7: Protocol fairness vs request distance

(number of S-D requests unfulfilled) are important measures of performance. In the results presented above, requests linger until satisfied, but it is unclear whether quantum applications can make use of entanglements much later than originally requested. Evaluations of previous protocols [2], [9] discard S-D requests if they cannot be satisfied immediately (one time slot), which leads to these protocols serving many low-hop count requests and essentially starving all others. Here, we explore the interaction between request latency, starvation rate, and S-D distance. For this set of results, we use a 200 node Waxman topology, $E_p = 0.5$, $q = 0.9$. We choose this setting because all three protocols achieve similar throughput in this setting. The QuARC results here use the generic 2D-grid thresholds, and are representative of using the topology-specific thresholds.

Figure 7(a) depicts the bias in request fulfillment as a function of distance. The y -axis shows the proportion of attempted requests that were successfully filled. Both Q-CAST and ALG-N-FUSION show a much stronger bias compared to QuARC in their ability to serve long requests, succeeding in fewer than 20% of requests longer than 8 hops. QuARC also experiences somewhat of a bias with distance; however this is by design. The red curve labeled “QuARC-1C” represents the highest achievable success rate when QuARC uses a single cluster. However, QuARC makes the decision to use multiple clusters in order to serve multiple concurrent S-D pairs, at the expense of a modest amount of distance-independence.

Figure 7(b) illustrates the effects of resource allocation bias. For each protocol and hop count, the plotted value is the ratio of the realized success rate (as shown in Figure 7(a)) to the maximum success rate. We measure the maximum success rate by supplying each protocol with a single S-D request at a time, isolating its fundamental ability to fill each request. Both Q-CAST and ALG-N-FUSION preferentially attempt to serve shorter requests, resulting in a significant reduction in efficiency of filling long-distance requests compared to their maximum capability. Meanwhile, QuARC’s FIFO queue prioritization allows for little choice in request selection, resulting in minimal bias or loss of efficiency when servicing multiple concurrent requests.

V. DISCUSSION

We discuss aspects of QuARC we have not covered, including ways in which QuARC’s adaptation can be improved.

A. QuARC Adaptation

As evaluated, QuARC’s adaptation scheme does not use any time-varying global information. We have experimented with providing QuARC with more global information. In particular, we have considered schemes which incorporate overall (global) success rate in addition to entanglement passing rate. Providing access to the global success rate did not result in substantial performance gains, and we opted for the simpler cluster-local metric.

It is likely that providing access to physical parameters, such as instantaneous p/q values (as is assumed in Q-CAST and ALG-N-FUSION), requested S-D path length distribution, etc., can lead to more effective cluster structures. Such a design needs to factor in the actual overhead of characterizing these parameters [28], [59] as well as the control overhead of distributing such information across the network.

Similarly, more advanced qubit assignment schemes may prove beneficial for throughput, but at the cost of additional overhead. QuARC’s approach allocates qubits in a distributed manner to try to maximize percolation benefit. However, it may be worthwhile to consider a scheme that allocates qubits on a request-specific basis to take advantage of specific topological features between a particular S-D pair. A more systematic study of this tradeoff is part of our future work.

B. Implementing QuARC

While our focus in this paper has been to introduce the idea of clustering in the context of quantum routing, we have also designed and implemented a fully distributed version of QuARC that resembles hierarchical link-state routing. Here, each cluster elects a leader through an election protocol, and the leader collects information about entanglement passing rate. The leader can then decide to initiate a split, or to initiate a merge by communicating the desire to merge with neighboring leaders. Individual S-D requests are source-routed (via the known cluster topology) in coordination with cluster leaders. The development of the necessary sub-protocols for robust leader election, leader-leader communication, time synchronization for initiating merges, and ordering of requests to be served was informed by corresponding classical concepts, which have been well-studied.

VI. CONCLUSION

We introduce QuARC, a new quantum routing protocol that uses dynamic clustering to simultaneously provide high throughput while decoupling performance from varying entanglement generation rates, swapping/fusion probabilities, and network size. QuARC does not use time-varying global information for clustering decisions, and our simulation-based evaluation shows that QuARC’s performance, both in terms of throughput, entanglement success rates, and request fulfillment latency, is robust with respect to dynamic changes in physical parameters.

REFERENCES

- [1] M. Pant, H. Krovi, D. Towsley, L. Tassiulas, L. Jiang, P. Basu, D. Englund, and S. Guha, "Routing entanglement in the quantum internet," *npj Quantum Information*, vol. 5, no. 1, p. 25, 2019.
- [2] S. Shi and C. Qian, "Concurrent entanglement routing for quantum networks: Model and designs," in *Proceedings of ACM SIGCOMM*, 2020, pp. 62–75. [Online]. Available: <https://doi.org/10.1145/3387514.3405853>
- [3] A. Patil, M. Pant, D. Englund, D. Towsley, and S. Guha, "Entanglement generation in a quantum network at distance-independent rate," *npj Quantum Information*, vol. 8, no. 1, p. 51, 2022.
- [4] A. Patil, J. I. Jacobson, E. Van Milligen, D. Towsley, and S. Guha, "Distance-independent entanglement generation in a quantum network using space-time multiplexed greenberger–horne–zeilinger (ghz) measurements," in *2021 IEEE International Conference on Quantum Computing and Engineering (QCE)*. IEEE, 2021, pp. 334–345.
- [5] S. Zhang, S. Shi, C. Qian, and K. L. Yeung, "Fragmentation-aware entanglement routing for quantum networks," *Journal of Lightwave Technology*, vol. 39, no. 14, pp. 4584–4591, 2021.
- [6] Y. Zhao, G. Zhao, and C. Qiao, "E2e fidelity aware routing and purification for throughput maximization in quantum networks," in *IEEE INFOCOM*, 2022, pp. 480–489.
- [7] Y. Zhao and C. Qiao, "Redundant entanglement provisioning and selection for throughput maximization in quantum networks," in *IEEE INFOCOM*, 2021, pp. 1–10.
- [8] Y. Zeng, J. Zhang, J. Liu, Z. Liu, and Y. Yang, "Multi-entanglement routing design over quantum networks," in *IEEE INFOCOM 2022-IEEE Conference on Computer Communications*. IEEE, 2022, pp. 510–519.
- [9] —, "Entanglement routing over quantum networks using greenberger-horne-zeilinger measurements," in *2023 IEEE 43rd International Conference on Distributed Computing Systems (ICDCS)*. IEEE, 2023, pp. 350–360.
- [10] E. Sutcliffe and A. Beghelli, "Multiuser entanglement distribution in quantum networks using multipath routing," *IEEE Transactions on Quantum Engineering*, vol. 4, no. 01, pp. 1–15, jan 2023.
- [11] W. K. Wootters and W. H. Zurek, "A single quantum cannot be cloned," *Nature*, vol. 299, no. 5886, pp. 802–803, 1982.
- [12] S. Pirandola, R. Laurenza, C. Ottaviani, and L. Bianchi, "Fundamental limits of repeaterless quantum communications," *Nature communications*, vol. 8, no. 1, p. 15043, 2017.
- [13] C. H. Bennett, G. Brassard, C. Crépeau, R. Jozsa, A. Peres, and W. K. Wootters, "Teleporting an unknown quantum state via dual classical and einstein-podolsky-rosen channels," *Physical review letters*, vol. 70, no. 13, p. 1895, 1993.
- [14] S. Wehner, D. Elkouss, and R. Hanson, "Quantum internet: A vision for the road ahead," *Science*, vol. 362, no. 6412, p. eaam9288, 2018.
- [15] H.-J. Briegel, W. Dür, J. I. Cirac, and P. Zoller, "Quantum repeaters: the role of imperfect local operations in quantum communication," *Physical Review Letters*, vol. 81, no. 26, p. 5932, 1998.
- [16] M. Zukowski, A. Zeilinger, M. Horne, and A. Ekert, "" event-ready-detectors" bell experiment via entanglement swapping," *Physical Review Letters*, vol. 71, no. 26, 1993.
- [17] J.-W. Pan, D. Bouwmeester, H. Weinfurter, and A. Zeilinger, "Experimental entanglement swapping: entangling photons that never interacted," *Physical review letters*, vol. 80, no. 18, p. 3891, 1998.
- [18] S. Olmschenk, D. Matsukevich, P. Maunz, D. Hayes, L.-M. Duan, and C. Monroe, "Quantum teleportation between distant matter qubits," *Science*, vol. 323, no. 5913, pp. 486–489, 2009.
- [19] M. Pompili, S. L. Hermans, S. Baier, H. K. Beukers, P. C. Humphreys, R. N. Schouten, R. F. Vermeulen, M. J. Tiggeleman, L. dos Santos Martins, B. Dirkse *et al.*, "Realization of a multinode quantum network of remote solid-state qubits," *Science*, vol. 372, no. 6539, pp. 259–264, 2021.
- [20] S. Hermans, M. Pompili, H. Beukers, S. Baier, J. Borregaard, and R. Hanson, "Qubit teleportation between non-neighbouring nodes in a quantum network," *Nature*, vol. 605, no. 7911, pp. 663–668, 2022.
- [21] J. Dynes, A. Wonfor, W.-S. Tam, A. Sharpe, R. Takahashi, M. Lucamarini, A. Pews, Z. Yuan, A. Dixon, J. Cho *et al.*, "Cambridge quantum network," *npj Quantum Information*, vol. 5, no. 1, p. 101, 2019.
- [22] J. Yin, Y. Cao, Y.-H. Li, S.-K. Liao, L. Zhang, J.-G. Ren, W.-Q. Cai, W.-Y. Liu, B. Li, H. Dai *et al.*, "Satellite-based entanglement distribution over 1200 kilometers," *Science*, vol. 356, no. 6343, pp. 1140–1144, 2017.
- [23] Y.-A. Chen, Q. Zhang, T.-Y. Chen, W.-Q. Cai, S.-K. Liao, J. Zhang, K. Chen, J. Yin, J.-G. Ren, Z. Chen *et al.*, "An integrated space-to-ground quantum communication network over 4,600 kilometres," *Nature*, vol. 589, no. 7841, pp. 214–219, 2021.
- [24] M. Sasaki, M. Fujiwara, H. Ishizuka, W. Klaus, K. Wakui, M. Takeoka, S. Miki, T. Yamashita, Z. Wang, A. Tanaka *et al.*, "Field test of quantum key distribution in the tokyo qkd network," *Optics express*, vol. 19, no. 11, pp. 10387–10409, 2011.
- [25] M. Peev, C. Pacher, R. Alléaume, C. Barreiro, J. Bouda, W. Boxleitner, T. Debuisschert, E. Diamanti, M. Dianati, J. Dynes *et al.*, "The secoqc quantum key distribution network in vienna," *New Journal of Physics*, vol. 11, no. 7, p. 075001, 2009.
- [26] T.-Y. Chen, X. Jiang, S.-B. Tang, L. Zhou, X. Yuan, H. Zhou, J. Wang, Y. Liu, L.-K. Chen, W.-Y. Liu *et al.*, "Implementation of a 46-node quantum metropolitan area network," *npj Quantum Information*, vol. 7, no. 1, p. 134, 2021.
- [27] E. Bersini, M. Grein, M. Sutula, R. Murphy, Y. Q. Huan, M. Stevens, A. Suleymanzade, C. Lee, R. Riedinger, D. J. Starling, P.-J. Stas, C. M. Knaut, N. Sinclair, D. R. Assumpcao, Y.-C. Wei, E. N. Knall, B. Machielse, D. D. Sukachev, D. S. Levonian, M. K. Bhaskar, M. Lončar, S. Hamilton, M. Lukin, D. Englund, and P. B. Dixon, "Development of a boston-area 50-km fiber quantum network testbed," *Phys. Rev. Appl.*, vol. 21, p. 014024, Jan 2024. [Online]. Available: <https://link.aps.org/doi/10.1103/PhysRevApplied.21.014024>
- [28] N. I. of Standards and T. (NIST), "Quantum Network Metrology at NIST," <https://www.nist.gov/pml/quantum-networks-nist/quantum-network-metrology>, 2022.
- [29] K. Fang, J. Zhao, X. Li, Y. Li, and R. Duan, "Quantum network: from theory to practice," *Science China Information Sciences*, vol. 66, no. 8, Jul. 2023. [Online]. Available: <http://dx.doi.org/10.1007/s11432-023-3773-4>
- [30] S. Pirandola, "End-to-end capacities of a quantum communication network," *Communications Physics*, vol. 2, no. 1, p. 51, 2019.
- [31] R. Van Meter, T. Satoh, T. D. Ladd, W. J. Munro, and K. Nemoto, "Path selection for quantum repeater networks," *Networking Science*, vol. 3, pp. 82–95, 2013.
- [32] W. Dai, T. Peng, and M. Z. Win, "Optimal remote entanglement distribution," *IEEE Journal on Selected Areas in Communications*, vol. 38, no. 3, pp. 540–556, 2020.
- [33] K. Chakraborty, D. Elkouss, B. Rijsman, and S. Wehner, "Entanglement distribution in a quantum network: A multicommodity flow-based approach," *IEEE Transactions on Quantum Engineering*, vol. 1, pp. 1–21, 2020.
- [34] L. Gyongyosi and S. Imre, "Decentralized base-graph routing for the quantum internet," *Physical Review A*, vol. 98, no. 2, p. 022310, 2018.
- [35] E. Schoute, L. Mancinska, T. Islam, I. Kerenidis, and S. Wehner, "Shortcuts to quantum network routing," *arXiv preprint arXiv:1610.05238*, 2016.
- [36] M. Caleffi, "Optimal routing for quantum networks," *Ieee Access*, vol. 5, pp. 22299–22312, 2017.
- [37] S. Das, S. Khatri, and J. P. Dowling, "Robust quantum network architectures and topologies for entanglement distribution," *Physical Review A*, vol. 97, no. 1, p. 012335, 2018.
- [38] K. Chakraborty, F. Rozpedek, A. Dahlberg, and S. Wehner, "Distributed routing in a quantum internet," *arXiv preprint arXiv:1907.11630*, 2019.
- [39] C. Li, T. Li, Y.-X. Liu, and P. Cappellaro, "Effective routing design for remote entanglement generation on quantum networks," *npj Quantum Information*, vol. 7, no. 1, p. 10, 2021.
- [40] H. Choi, M. G. Davis, Á. G. Iñesta, and D. R. Englund, "Scalable quantum networks: Congestion-free hierarchical entanglement routing with error correction," *arXiv preprint arXiv:2306.09216*, 2023.
- [41] C. Cicconetti, M. Conti, and A. Passarella, "Request scheduling in quantum networks," *IEEE Transactions on Quantum Engineering*, vol. 2, pp. 2–17, 2021.
- [42] P. Dhara, A. Patil, H. Krovi, and S. Guha, "Subexponential rate versus distance with time-multiplexed quantum repeaters," *Physical Review A*, vol. 104, no. 5, p. 052612, 2021.
- [43] A. Farahbakhsh and C. Feng, "Opportunistic routing in quantum networks," in *IEEE INFOCOM 2022-IEEE Conference on Computer Communications*. IEEE, 2022, pp. 490–499.
- [44] Y. Gan, X. Zhang, R. Zhou, Y. Liu, and C. Qian, "A routing framework for quantum entanglements with heterogeneous duration," in *2023 IEEE International Conference on Quantum Computing and Engineering (QCE)*, vol. 1. IEEE, 2023, pp. 1132–1142.

- [45] E. Kaur and S. Guha, "Distribution of entanglement in two-dimensional square grid network," in *2023 IEEE International Conference on Quantum Computing and Engineering (QCE)*, vol. 1. IEEE, 2023, pp. 1154–1164.
- [46] A. Dahlberg, M. Skrzypczyk, T. Coopmans, L. Wubben, F. Rozpędek, M. Pompili, A. Stolk, P. Pawełczak, R. Knegjens, J. de Oliveira Filho *et al.*, "A link layer protocol for quantum networks," in *Proceedings of the ACM special interest group on data communication*, 2019, pp. 159–173.
- [47] H. Bernien, B. Hensen, W. Pfaff, G. Koolstra, M. S. Blok, L. Robledo, T. H. Taminiau, M. Markham, D. J. Twitchen, L. Childress *et al.*, "Heralded entanglement between solid-state qubits separated by three metres," *Nature*, vol. 497, no. 7447, pp. 86–90, 2013.
- [48] Q. Zhuang and B. Zhang, "Quantum communication capacity transition of complex quantum networks," *Physical Review A*, vol. 104, no. 2, p. 022608, 2021.
- [49] O. Malik, X. Meng, S. Havlin, G. Korniss, B. K. Szymanski, and J. Gao, "Concurrence percolation threshold of large-scale quantum networks," *Communications Physics*, vol. 5, no. 1, p. 193, 2022.
- [50] M. Girvan and M. E. Newman, "Community structure in social and biological networks," *Proceedings of the national academy of sciences*, vol. 99, no. 12, pp. 7821–7826, 2002.
- [51] M. Li, R.-R. Liu, L. LÄŒ, M.-B. Hu, S. Xu, and Y.-C. Zhang, "Percolation on complex networks: Theory and application," *Physics Reports*, vol. 907, pp. 1–68, 2021, percolation on complex networks: Theory and application. [Online]. Available: <https://www.sciencedirect.com/science/article/pii/S0370157320304269>
- [52] J. G. Kemeny and J. L. Snell, *Finite markov chains*. New York Springer-Verlag, 1983, originally published: Princeton, N.J. : Van Nostrand, 1960.
- [53] S. Cao, B. Wu, F. Chen, M. Gong, Y. Wu, Y. Ye, C. Zha, H. Qian, C. Ying, S. Guo, Q. Zhu, H.-L. Huang, Y. Zhao, S. Li, S. Wang, J. Yu, D. Fan, D. Wu, H. Su, H. Deng, H. Rong, Y. Li, K. Zhang, T.-H. Chung, F. Liang, J. Lin, Y. Xu, L. Sun, C. Guo, N. Li, Y.-H. Huo, C.-Z. Peng, C.-Y. Lu, X. Yuan, X. Zhu, and J.-W. Pan, "Generation of genuine entanglement up to 51 superconducting qubits," *Nature*, vol. 619, no. 7971, pp. 738–742, 2023.
- [54] Z. Zhang and Q. Zhuang, "Distributed quantum sensing," *Quantum Science and Technology*, vol. 6, no. 4, p. 043001, jul 2021. [Online]. Available: <https://dx.doi.org/10.1088/2058-9565/abd4c3>
- [55] D. Gottesman, T. Jennewein, and S. Croke, "Longer-baseline telescopes using quantum repeaters," *Phys. Rev. Lett.*, vol. 109, p. 070503, Aug 2012. [Online]. Available: <https://link.aps.org/doi/10.1103/PhysRevLett.109.070503>
- [56] B. M. Waxman, "Routing of multipoint connections," *IEEE journal on selected areas in communications*, vol. 6, no. 9, pp. 1617–1622, 1988.
- [57] "Source code for q-cast quantum routing simulations," 2019. [Online]. Available: <https://github.com/QianLabUCSC/QuantumRouting>.
- [58] "Source code for quarc: cluster-based routing on quantum networks," 2024. [Online]. Available: <https://github.com/cbclayton/clustered-quantum-routing>.
- [59] J. Helsen and S. Wehner, "A benchmarking procedure for quantum networks," *npj Quantum Information*, vol. 9, no. 1, p. 17, 2023.